ACS APPLIED ELECTRONIC MATERIALS

pubs.acs.org/acsaelm

Article

From Donor−Donor Exciplex-Forming Interfaces to Detection of an Explosive Compound with Phenylethenyl Derivatives Redefining OLED Efficiency and Extremely High Sensitivity to Picric Acid

Ehsan Ullah Rashid, Monika Cekaviciute, Jurate Simokaitiene, Melika Ghasemi, Dmytro Volyniuk, Khrystyna Ivaniuk, Pavlo Stakhira, and Juozas Vidas Grazulevicius*

Cite This: https://doi.org/10.1021/acsaelm.5c00123

Read Online

ACCESS | Metrics & More | Article Recommendations | Supporting Information

ABSTRACT: In this study, three derivatives of phenylethenyl-substituted phenoxazine and phenothiazine are synthesized via Buchwald-Hartwig cross-coupling, targeting multifunctionality as exciplex-forming materials and efficient cyan emitters for organic light-emitting diodes (OLEDs) and sensitive dectectors of picric acid. Advanced density functional theory (DFT) calculations at the mPW1PW91/6−31G(d,p) level unveil the intricate electronic architectures of these compounds, emphasizing their spatial molecular orbitals and the charge-transfer dynamics governing excited-state properties. Reorganization energy calculations indicate superior hole mobility, particularly for derivatives with tetraphenylethenyl groups. Photophysical investigations reveal aggregation-induced emission enhancement (AIEE) in water-THF mixtures, with cyan fluorescence intensifying at high water fractions (f_w% = 99) due to the formation of emissive aggregates. Photoluminescence quantum yields (PLQYs) are significantly higher of solid films (13.5−53%) compared to those of dilute toluene solutions (3−26%). This observation is attributed to enhanced intermolecular interactions and aggregate formation. The emissive aggregates of the compounds exhibit extremely high sensitivity to electron-deficient picric acid via noncovalent interactions with Stern−Volmer constants up to 2.96 × 10^4 M^{-1}. This is attributed to their strong donor−acceptor charge-transfer mechanisms. OLEDs employing these materials as emitters display bluish-cyan electroluminescence (λ_{max}≈500 nm), with brightness surpassing 1000 cd/m^2 and external quantum efficiencies (EQEs) ranging from 2.5 to 6%. The relatively high EQEs are explained by triplet harvesting from interface donor−donor exciplexes.

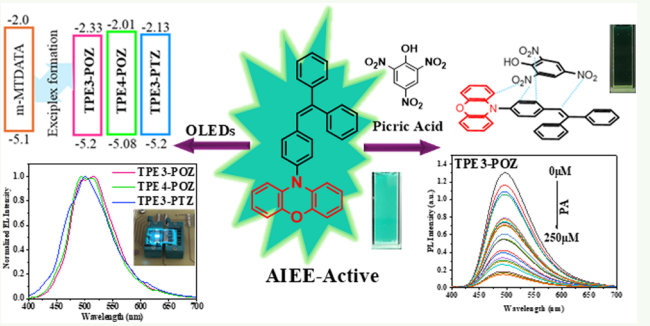

KEYWORDS: *phenoxazine, phenothiazine, tetraphenylethylene, aggregation-induced emission enhancement, exciplex, picric acid sensing, doping-free organic light-emitting diode*

1. INTRODUCTION

Organic light-emitting diodes (OLEDs) have emerged as transformative devices, driven by their exceptional emissive properties, flexible display potential, and energy efficiency.[1−3] However, the practical implementation of organic semiconductors in thin films faces the challenge of aggregation-caused quenching (ACQ), wherein molecular aggregation suppresses fluorescence due to nonradiative pathways.[4] This limitation, prevalent in many aromatic compounds, results in high-intensity fluorescence of dilute solutions but weak or quenched emission of the concentrated forms.[5,6] The advent of aggregation-induced emission (AIE), first identified by Tang et al. in 2001 using silole-based systems,[7] revolutionized this paradigm. Unlike ACQ, AIE-active materials exhibit enhanced emission in aggregated states.[8] This phenomenon, further refined as aggregation-induced emission enhancement (AIEE), highlights a subclass of molecules that retain high fluorescence across solution, solid, and aggregated states due to restricted intramolecular motions, limiting nonradiative energy dissipation.[9]

Building on these insights, the incorporation of azaanthracene derivatives such as phenoxazine and phenothiazine has gained significant traction in materials science due to their unique electronic structures and superior photophysical properties.[10] Derivatives with tri- and tetraphenylethylene moieties have demonstrated AIEE, with enhanced emission intensities and high photoluminescence quantum yields (PLQYs) in solid-state films, making them ideal candidates for host-free OLEDs[11,12] Emission of these chromophores

Received: January 20, 2025
Revised: April 2, 2025
Accepted: April 3, 2025

Scheme 1. Synthesis of Compounds TPE3-POZ, TPE3-PTZ, and TPE4-POZ[a]

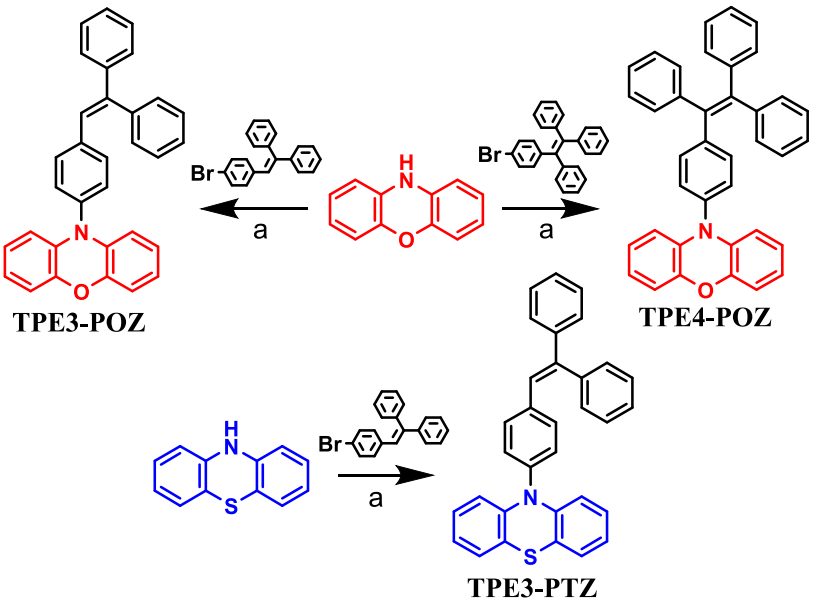

[a](a) NaOt-Bu, $Pd(OAc)_3$, $P(t\text{-}Bu)_3$, anhydrous toluene, reflux.

overcome ACQ effects.[13,14] They exhibit vibrant blue or sky blue fluorescence owing to their twisted geometries and rotationally unrestricted groups, which reduce molecular $\pi-\pi$ stacking interactions in aggregated states.[15] The recent studies underscore the synthesis of high-yield phenylethylene-based emitters, showcasing PLQYs of 26−53% of the films of neat compounds and external quantum efficiencies (EQEs) of OLEDs of up to 1.59%.[16] They emit in the range of wavelengths of 451−481 nm. Notably, diphenylethylene-substituted phenoxazine and phenothiazine derivatives, synthesized by Huang et al. in 2020, exhibit AIEE attributed to their highly twisted architectures.[10] This structural feature, induced by the rotational degrees of freedom in diphenylethylene groups, suppresses nonradiative relaxation pathways and facilitates efficient radiative transitions.

Organic luminophores exhibiting robust aggregate-state emission are exceptionally suited for the detection of picric acid, a highly electron-deficient nitroaromatic compound of significant environmental and explosive relevance.[17] The electron-deficient nature of nitroaromatic compounds facilitates their interaction with electron-rich fluorophores via a photoinduced electron transfer (PET) mechanism, effectively modulating the emissive properties of the fluorescent probes. In aggregated states, the dense packing of electron-rich luminophores promotes noncovalent interactions with picric acid through charge-transfer processes, leading to pronounced fluorescence quenching. This quenching is indicative of the strong donor−acceptor interplay, making such luminophores highly effective in achieving ultrasensitive detection of nitroaromatic analytes.[18,19]

In this study, three derivatives of triphenylethylene conjugated with phenoxazine (**TPE3-POZ**) and phenothiazine (**TPE3-PTZ**), along with tetraphenylethylene-substituted phenoxazine (**TPE4-POZ**) were synthesized using a single-step Buchwald-Hartwig coupling methodology. The comprehensive investigations encompassing both density functional theory (DFT) computations and experimental photophysical analyses were conducted to unravel the intricate optical and electronic properties of the compounds. Electrochemical characteristics were elucidated through cyclic voltammetry ($C-V$), while thermal stability and phase transitions were assessed using thermogravimetric analysis (TGA) and differential scanning calorimetry (DSC), respectively. The presence of rotatable tri/tetraphenylethylene moieties induces pronounced molecular twisting, fostering AIEE, high PLQY, and the development of cyan-emitting host-free OLEDs with efficiency enhancement via interface exciplex formation. Despite the weak electron-donating abilities of the developed compounds, they form exciplexes with electron-donating compound, 4,4′,4″-tris[phenyl(m-tolyl)amino]triphenylamine (m-MTDATA).[20] Donor−acceptor exciplex-forming molecular mixtures are widely used as hosts or emitters for the enhancement of OLED efficiency.[21−23] To the best of our knowledge, the donor−donor exciplex formation has not been discovered yet. This finding opens new possibilities for the design of OLEDs. Furthermore, the electron-rich nature of these luminophores enabled ultrasensitive detection of the electron-deficient nitroaromatic picric acid via a charge-transfer-mediated fluorescence quenching mechanism, underscoring their multifunctional applicability.

2. RESULTS AND DISCUSSION

2.1. Synthesis. Scheme 1 shows the synthetic approach to the desired derivatives. Compounds **TPE3-POZ**, **TPE3-PTZ**, and **TPE4-POZ** were synthesized using a one-step procedure, namely, the Buchwald-Hartwig method in the presence of palladium complex[24,25] The synthesized compounds were identified by mass spectrometry, infrared spectroscopy, and nuclear magnetic resonance (^1H, ^{13}C) spectroscopy.

2.2. Thermal Properties. High thermal resilience of the compounds and robust morphological integrity of their layers are critical prerequisites for electroactive materials intended for OLED applications, ensuring long-term stability of their functional layers. To assess the thermal endurance and potential morphological transitions of the synthesized derivatives of phenoxazine and phenothiazine, thermogravimetric

https://doi.org/10.1021/acsaelm.5c00123
ACS Appl. Electron. Mater. XXXX, XXX, XXX−XXX

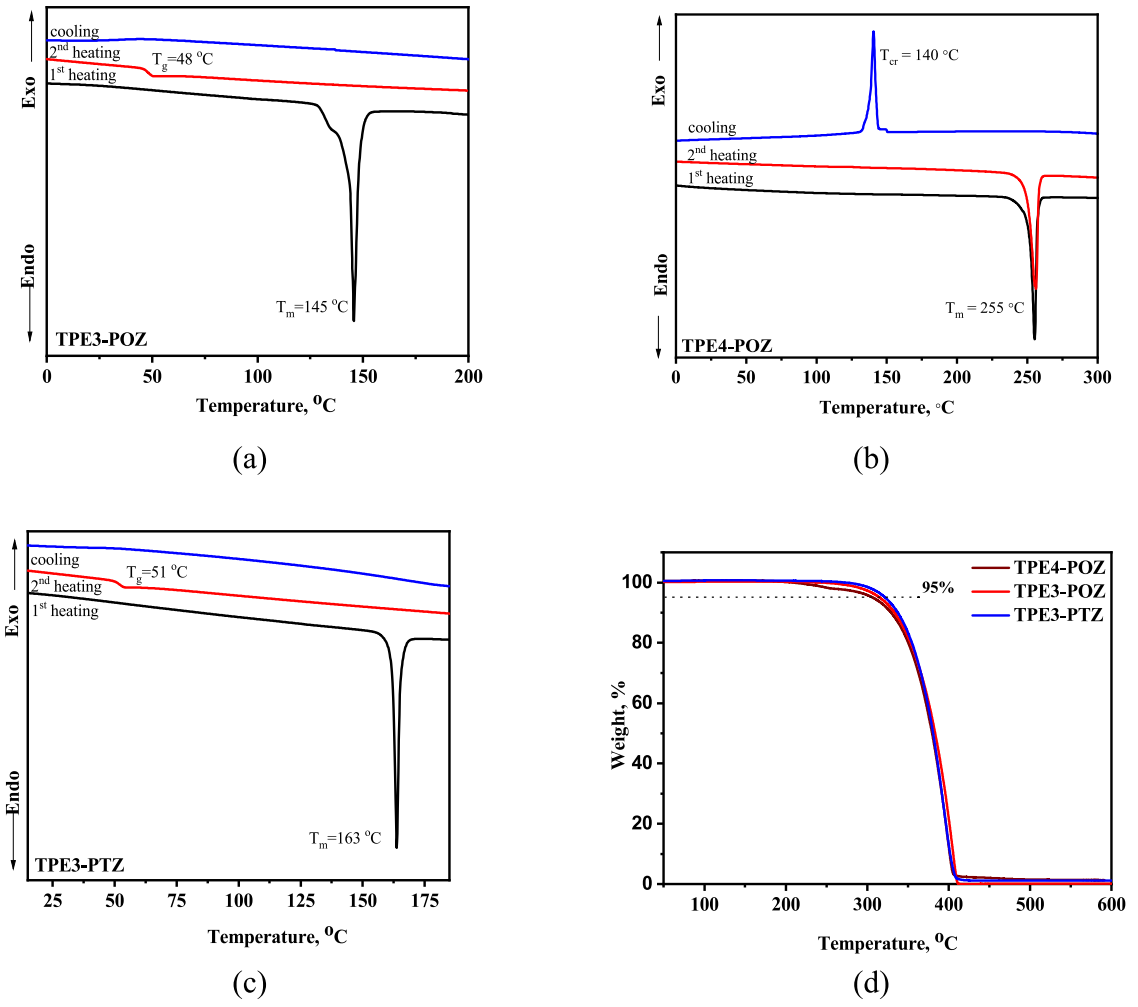

Figure 1. DSC (a–c) and TGA (d) curves of compounds **TPE3-POZ**, **TPE3-PTZ**, and **TPE4-POZ**.

Table 1. Thermal, Electrochemical and Photoelectrical Characteristics of TPE3-POZ, TPE3-PTZ, and TPE4-POZ[a]

compound	T_{cr}, °C	T_g, °C	T_m, °C	$T_d^{5\%}$, °C	$^aE_g^{opt}$, eV	E_{ox}^{onset}, V	IP^{CV}, eV	EA^{CV}, eV	IP^{PE}, eV	$^bE_g^{opt}$, eV	EA^{PE}, eV
TPE3-POZ		48	145	315	2.91	0.33	5.13	2.22	5.2	2.87	2.33
TPE4-POZ	140		255	306	3.07	0.51	5.31	2.24	5.08	3.07	2.01
TPE3-PTZ		51	163	322	3.11	0.39	5.19	2.08	5.2	3.07	2.13

[a]Crystallization temperature (T_{cr}), glass transition temperatures (T_g), and melting points (T_m) were measured by DSC (heating rate of 10 °C/min under nitrogen atmosphere). 5% weight loss temperatures ($T_d^{5\%}$) were estimated by TGA (heating rate of 20 °C/min under nitrogen atmosphere). The optical band gap ($^aE_g^{opt}$) estimated from the edges of absorption spectra of toluene solutions ($E_g^{opt} = 1240/\lambda_{onset}$). Oxidation onset ($E_{ox}^{onset}$). Ionization potentials (IP^{CV}) and electron affinity (EA^{CV}). Photoelectron emission (PE) spectroscopy used for the determination of ionization potential (IP^{PE}) and electron affinities (EA^{PE}) of solid samples. The optical band gap ($^bE_g^{opt}$) estimated from the edges of absorption spectra of solid samples ($E_g^{opt} = 1240/\lambda_{onset}$).

analysis (TGA) and differential scanning calorimetry (DSC) were employed (Figure 1). The thermal characterization of the compounds was carried out under nitrogen atmosphere. All of the synthesized compounds showed single-step weight loss with moderately high temperatures of the onsets of weight loss. The temperatures of five percent weight loss ($T_d^{5\%}$) were quite close. They ranged from 306 to 322 °C, as confirmed by TGA at the heating rate of 20 °C/min (Table 1). The single-step complete weight losses observed during TGA experiments indicate that these temperatures are rather of the onsets of the sublimation but not of the thermal degradation.

All synthesized compounds were obtained as crystalline solids, exhibiting melting temperatures (T_m) in the first DSC heating scans within the range of 145–255 °C. Notably, the triphenylethenyl-containing derivatives **TPE3-POZ** and **TPE3-PTZ** displayed significantly lower melting points (of 145 and 163 °C, respectively) compared to **TPE4-POZ** having tetraphenylethenyl moieties, which exhibited a higher melting point of 255 °C.[26] **TPE3-POZ** and **TPE3-PTZ** with triphenylethenyl moieties formed molecular glasses. They were characterized by glass transition temperatures (T_g) of 48 and 51 °C, respectively (Table 1). These molecular glasses demonstrated enhanced morphological stability, as no tendency for crystallization was observed during subsequent thermal cycles in the DSC experiments. In contrast, **TPE4-POZ**, containing the more rigid tetraphenylethenyl group, did not exhibit glass formation. Instead, an exothermic crystallization signal was detected at 140 °C, indicating a strong

https://doi.org/10.1021/acsaelm.5c00123
ACS Appl. Electron. Mater. XXXX, XXX, XXX–XXX

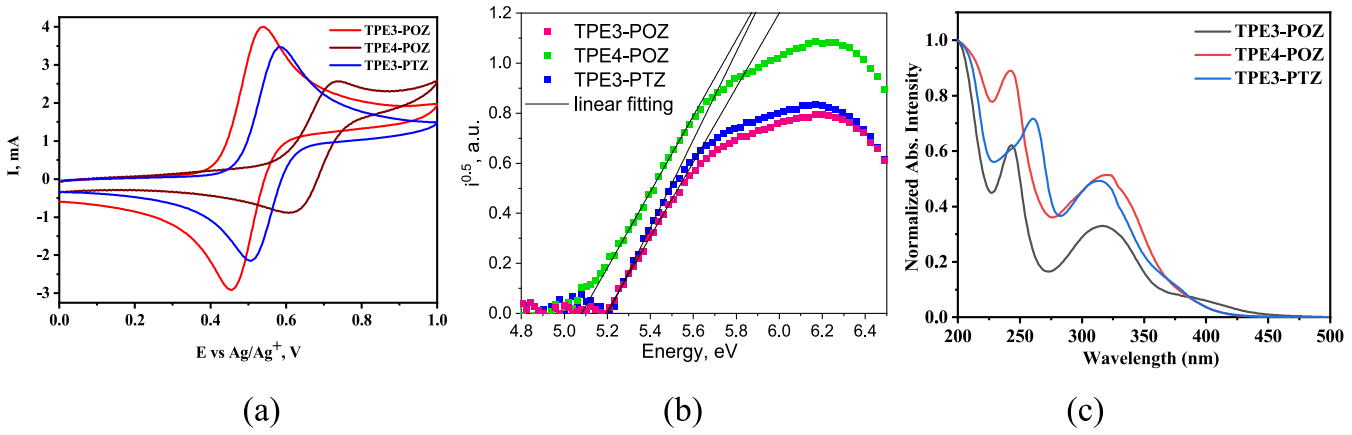

Figure 2. First *C*−*V* cycle curves (a) of dilute solutions of **TPE3-POZ, TPE3-PTZ**, and **TPE4-POZ** in dichloromethane (room temperature) recorded at a sweep rate of 0.1 V/s. Photoelectron emission (b) and absorption (c) spectra of solution-processed films of **TPE3-POZ, TPE3-PTZ**, and **TPE4-POZ**.

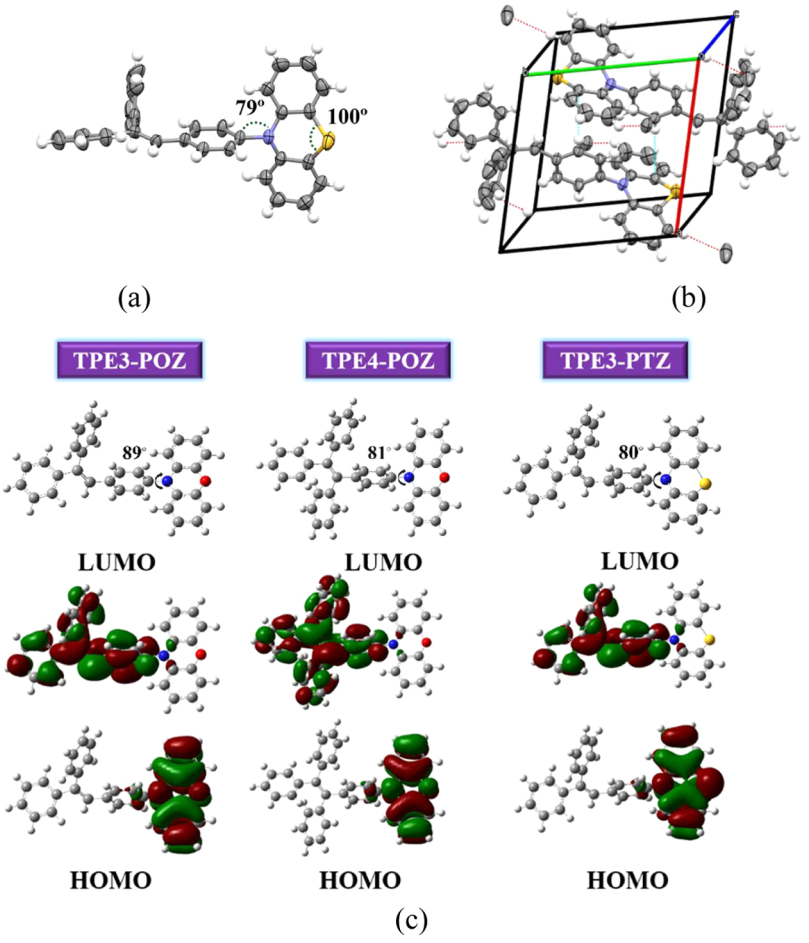

Figure 3. Single-crystal X-ray structure (a), packing pattern in the crystal lattice of **TPE3-PTZ** (b), optimized electronic structures and molecular orbitals of **TPE3-POZ, TPE4-POZ**, and **TPE3-PTZ** (c).

propensity for reorganization into the crystalline phase upon cooling.

2.3. Electrochemical Properties. The electrochemical properties of the synthesized compounds were investigated using cyclic voltammetry (*C*−*V*). The cyclic voltammograms exhibited well-defined, reversible oxidation processes, with anodic and cathodic peak currents showing equal magnitudes and a linear dependence on the sweep rate. This observation confirms the diffusion-controlled nature of the electron transfer process (Figure 2). The oxidation onset potentials (E_{ox}^{onset}) were referenced against ferrocene (Fc). The ionization potential (IP^{CV}) values were determined using the relationship $IP^{CV} = 4.8 + E_{ox}^{onset}$. The IP^{CV} values of the compounds ranged between 5.13 and 5.31 eV. Among the derivatives, the tetraphenylethenyl-containing compound **TPE4-POZ** exhibited the highest IP value (5.31 eV), which suggests

https://doi.org/10.1021/acsaelm.5c00123
ACS Appl. Electron. Mater. XXXX, XXX, XXX−XXX

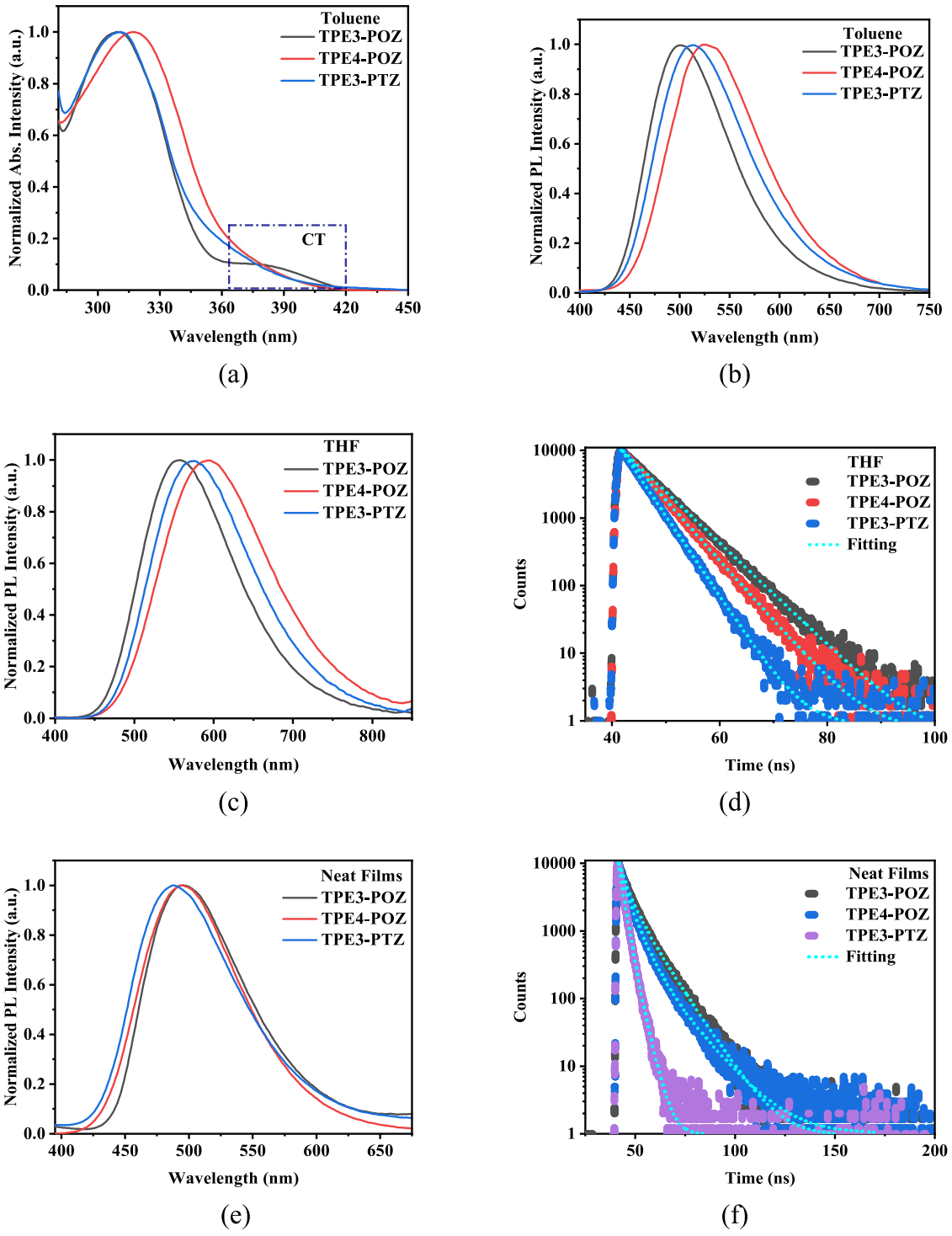

Figure 4. (a) UV−vis absorption spectra of toluene solutions (conc. 10^{-5} M). (b) PL spectra of toluene solutions, (c and d) PL spectra and PL decay curves of THF solutions. (e, f) PL spectra and PL decay curves of neat films of **TPE3-POZ**, **TPE4-POZ**, and **TPE3-PTZ**.

increased destabilization of the ionization energy. The triphenylethenyl-containing compounds, **TPE3-POZ** and **TPE3-PTZ**, displayed comparatively lower IP values of 5.13 and 5.19 eV, respectively. The electron affinity (EA^{CV}) of the compounds was estimated based on the energies of their optical band gaps (E_g^{opt}) and IP^{CV} values. They were calculated using the equation $EA^{CV} = IP^{CV} - E_g^{opt}$.[27] Compound **TPE3-PTZ**, incorporating phenothiazine moiety, exhibited the most stabilized electron affinity (2.08 eV). The tetraphenylethenyl-containing compound **TPE4-POZ** showed a slightly higher EA value (2.24 eV) compared to that of **TPE3-POZ**. This observation indicates a marginal destabilization of EA induced by the tetraphenylethenyl moiety.

For the prediction of exciplex-forming properties and the design of electroluminescent devices, the determination of the charge transport energy levels of the solid films of organic semiconductors is required.[28] With this request, we used photoelectron emission (PE) spectroscopy to determine the

https://doi.org/10.1021/acsaelm.5c00123
ACS Appl. Electron. Mater. XXXX, XXX, XXX−XXX

ionization potential (I_P^{PE}) and electron affinities (E_A^{PE}) of solution-processed films of **TPE3-POZ, TPE3-PTZ,** and **TPE4-POZ** (Figure 2b). The I_P^{PE} values of **TPE3-POZ, TPE3-PTZ,** and **TPE4-POZ** were found to be 5.2, 5.2, and 5.08 eV, respectively (Table 1). The triphenylethenyl-containing compounds, **TPE3-POZ** and **TPE3-PTZ,** displayed higher I_P^{PE} values than tetraphenylethenyl-containing compound **TPE4-POZ**. The nature of donor moieties (phenoxazine vs phenothiazine) does not affect the I_P^{PE} values of **TPE3-POZ** and **TPE3-PTZ**. This observation is in good agreement with the results of the above-described $C-V$ measurements. The low I_P^{PE} values of **TPE3-POZ, TPE3-PTZ,** and **TPE4-POZ** ensure injection of holes from the indium tin oxide (**ITO**) electrode without using additional layers. The electron affinity (E_A^{PE}) values of the films were estimated using the formula $E_A^{PE} = I_P^{PE} - E_g^{opt}$. The optical band gaps (E_g^{opt}) of 2.87, 3.07, and 3.07 eV were obtained using the offsets of low-energy bands of the absorption spectra of the films of **TPE3-POZ, TPE3-PTZ,** and **TPE4-POZ,** respectively (Figure 2c). The E_A^{PES} values of **TPE3-POZ, TPE3-PTZ,** and **TPE4-POZ** were found to be 2.33, 2.13, and 2.01 eV, respectively (Table 1).

2.4. Single-Crystal X-ray Analysis. A single crystal of **TPE3-PTZ** was successfully grown, and its structural elucidation was performed through single-crystal X-ray analysis to gain profound insights into its geometric and packing characteristics. The crystallographic analysis revealed that **TPE3-PTZ** crystallizes in the triclinic crystal system, adopting the P $\bar{1}$ (2) space group. The comprehensive crystallographic parameters are detailed in Table S1. The structural investigations revealed a significant dihedral twist of ca. **79°** between the triphenylethylene and phenothiazine units, underscoring a highly twisted molecular conformation (Figure 1a). Additionally, the C−S−C bond angle in the phenothiazine core was measured to be ca. 100°, indicating a mild structural bending within this rigid heterocyclic moiety. This pronounced torsional distortion and intrinsic bending effectively preclude strong $\pi-\pi$ stacking interactions, which is further corroborated by the packing analysis. Despite the absence of classical $\pi-\pi$ interactions, a detailed examination of the crystal packing reveals the presence of multiple short contacts contributing to the intermolecular stabilization (Figure 1b). Notably, alternating moieties within the lattice interact via C−H***π interactions, where the triphenylethylene unit of one molecule engages with the phenothiazine unit of an adjacent molecule. The specific short contact distances include (TPE3)C−H***π(PTZ) at 2.83 Å, along with two additional (PTZ)C−H***π(TPE3) interactions at 2.88 and 2.82 Å.

2.5. Density Functional Theory Calculations. The electronic structures of **TPE3-POZ, TPE3-PTZ,** and **TPE4-POZ** optimized at mPW1PW91/6−31G(d,p) level using DFT approach. To evaluate the degree of orbital delocalization and charge separation, the spatial twists between the key molecular moieties were analyzed (Figure 3c). The dihedral angles between the phenoxazine, phenothiazine, and tri/tetraphenylethenyl units were found to lie within the range of 80−89°, indicating a near-orthogonal orientation of the moieties. This pronounced twist suggests significant charge separation between the frontier molecular orbitals. It is further evidenced by the visualized distributions of the highest occupied molecular orbital (HOMO) and the lowest unoccupied molecular orbital (LUMO) (Figure 3c). The HOMO was predominantly localized on the phenoxazine moiety in **TPE3-POZ** and **TPE4-POZ** and on the phenothiazine core in TPE3-PTZ, whereas the LUMO was primarily situated on the tri/tetraphenylethenyl fragments. Such highly twisted geometries facilitate notable charge separation while still maintaining minimal orbital overlap, as evidenced by the small degree of charge density overlap between the HOMO and LUMO. To quantitatively analyze the contributions of the individual molecular components to the HOMO and LUMO, a density of states (DOS) analysis was performed using Mulliken's charge density method. The graphical representation of the DOS analysis is presented in Figure S1. The corresponding numerical data are summarized in Table S2. The results revealed that the HOMO exhibits dominant contributions from the phenoxazine and phenothiazine moieties, with only a minute contribution from the tri/tetraphenylethenyl units. Conversely, the LUMO showed substantial contributions from the tri/tetraphenylethenyl moieties, with minor participation from the phenoxazine and phenothiazine units. This observed trend in DOS analysis further corroborates the charge separation. The predominant contributions highlight the spatial segregation of electron density, while the minimal contributions reflect a slight but significant overlap of molecular orbitals. The intramolecular reorganization energy for hole transport (λ_h) offers critical insights into the hole mobility of the investigated compounds, revealing their exceptional hole-transporting potential. Given the inverse correlation between λ_h and charge mobility, lower reorganization energy inherently translates to enhanced charge-carrier mobility.[29] Among the derivatives, **TPE3-POZ** and **TPE4-POZ** demonstrated practically identical λ_h values of 0.215 and 0.214 eV, respectively, signifying superior hole mobility. **TPE3-PTZ** exhibited a significantly higher λ_h of 0.531 eV, indicating comparatively inferior hole-transporting efficiency. Notably, **TPE4-POZ**, featuring the tetraphenylethylene moiety, exhibited slightly enhanced hole mobility due to its marginally lower λ_h compared to that of **TPE3-POZ**.

2.6. Photophysical Properties. The absorption spectra of the solutions of the synthesized compounds in toluene (Figure 4a) reveal intense absorption bands centered at ca. 310 nm. They correspond to the $\pi-\pi^*$ transitions localized on the triphenylethenyl moiety of **TPE3-POZ** and **TPE3-PTZ**. A slight red shift to ca. 317 nm is observed in the case of the solution of **TPE4-POZ**. It is attributed to the $\pi-\pi^*$ transition of the tetraphenylethenyl moiety.[30] This red shift is a direct consequence of the increased conjugation provided by the additional phenyl ring in tetraphenylethenyl compared to triphenylethenyl. To gain deeper insights into the excited-state properties and electronic transitions, time-dependent DFT (TD-DFT) calculations were performed. The computed absorption spectra are presented in Figure S2. The detailed excited-state characteristics are summarized in Table S3. TD-DFT analysis identifies the high-energy absorption band for all of the studied compounds as originating from the S_3 state, which corresponds to the HOMO−1→LUMO transition (Figure S3). This transition is primarily localized on the triphenylethenyl moiety of **TPE3-POZ** and **TPE3-PTZ**, while for **TPE4-POZ**, it is associated with the tetraphenylethenyl moiety. The observed red shift in the absorption band with the extension from tri- to tetraphenylethenyl is further corroborated by TD-DFT results, highlighting the influence of the enhanced conjugation.

The S_2 state, characterized by negligible oscillator strength, corresponds to the HOMO→LUMO+1 transition, indicating electron localization on the phenoxazine or phenothiazine

https://doi.org/10.1021/acsaelm.5c00123
ACS Appl. Electron. Mater. XXXX, XXX, XXX−XXX

Table 2. Photophysical Properties of TPE3-POZ, TPE3-PTZ, and TPE4-POZ

compound	toluene			THF		film		
	λ_{abs}^{max}, nm	λ_{PL}^{max}, nm	PLQY, %	λ_{PL}^{max}, nm	τ, ns	λ_{PL}^{max}, nm	τ, ns	PLQY, %
TPE3-POZ	310	500	26	556	5.7	495	7.4	53
TPE4-POZ	317	527	3	593	4.8	494	6.2	13.5
TPE3-PTZ	310	513	4	574	3.6	488	2.5	5.25

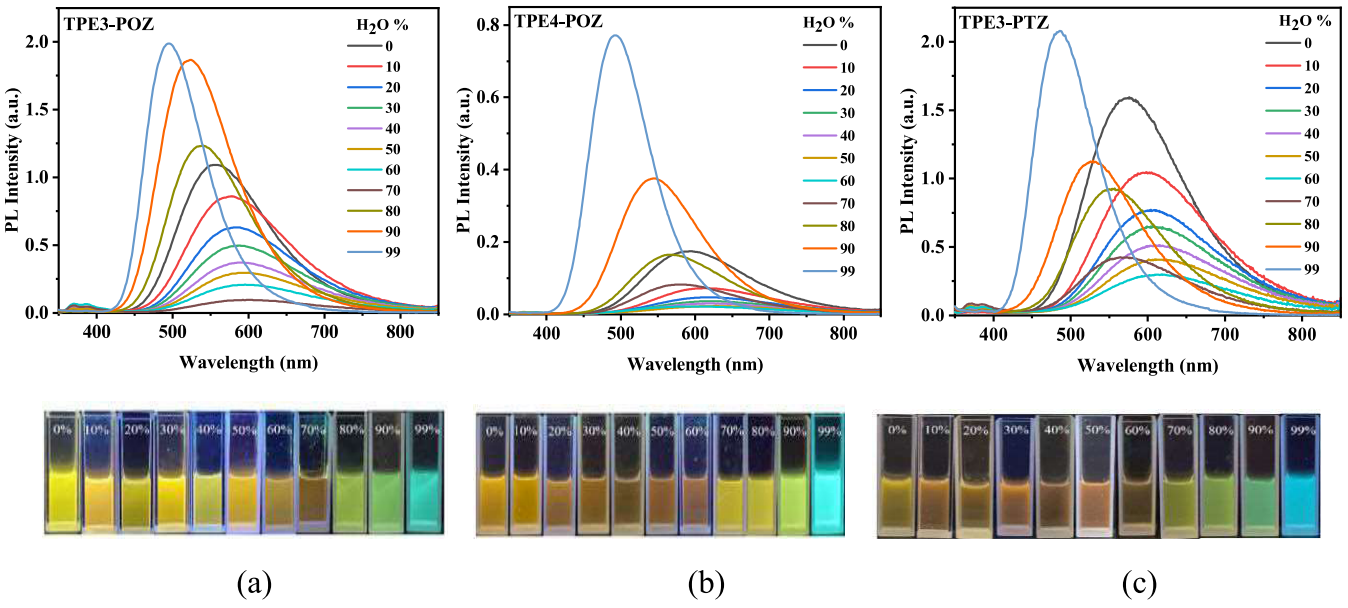

Figure 5. PL spectra of the dispersions of **TPE3-POZ** (a), **TPE3-PTZ** (b), and **TPE4-POZ** (c) in the mixtures of THF and water with 0−99% water fractions and the photographs of the dispersions under UV light.

moieties with a subsequent charge transfer (CT) to the tri/tetraphenylethenyl moiety. Importantly, the TD-DFT computations also reveal the presence of a low-energy S_1 state for all of the compounds, representing the HOMO→LUMO transition. This transition reflects a pronounced CT from the electron-donating phenoxazine (in **TPE3-POZ** and **TPE4-POZ**) and phenothiazine (in **TPE3-PTZ**) moieties to the electron-accepting tri/tetraphenylethenyl units. Due to the nearly orthogonal geometry between the donor and acceptor moieties, the S_1 state exhibits minimal oscillator strength, resulting in a weak absorption band. The experimental investigations show a weak but more pronounced absorption band at ca.390 nm for the toluene solutions of **TPE4-POZ** (Figure 4a) compared to those of **TPE3-POZ** and **TPE3-PTZ**. This is attributed to a slightly smaller dihedral angle between the tetraphenylethenyl and phenoxazine moieties, enhancing coupling and increasing the oscillator strength of the CT transition.[31]

The photoluminescence (PL) spectra of dilute toluene and THF solutions of the compounds were recorded. The single emission bands with the intensity maxima at ca.500−527 nm were observed for toluene solutions and at ca. 556−593 nm for THF solutions (Figure 4b,c, Table 2). The pronounced red shift observed for THF solutions compared to toluene solutions of the compounds highlights the polarity-dependent nature of the emission. It is an indication of a CT excited state, consistent with TD-DFT predictions. The presence of the tetraphenylethenyl moiety in **TPE4-POZ** further induces a red shift in both absorption and emission spectra, making its PL spectra the most red-shifted among the compounds. The PL decay curves of the THF solutions (Figure 4d) revealed rapid fluorescence with lifetimes ranging from 3.6−5.7 ns, characteristic of the fast radiative decay processes. Notably, the PL spectra of neat films exhibited a significant blue shift relative to the solution spectra, with the maxima constrained to a narrow range of 488−495 nm (Figure 4e). The blue shifts of emission of the solid films with respect to those of toluene and THF solutions can be attributed to the extreme sensitivity of the intramolecular CT state to the polarity of the surrounding medium. In toluene solution, the weakly polar environment provides limited stabilization of the intramolecular CT state, resulting in a modest red shift relative to the solid-state emission. However, in the solution of more polar THF, enhanced stabilization of the CT state further lowers its energy, leading to a more pronounced red shift. Conversely, in the solid film, the absence of a polar solvent environment leads to destabilization of the intramolecular CT state, and the blue shift of the emission peak. The PL lifetimes of solid films of **TPE3-POZ** and **TPE4-POZ** were found to be slightly higher (7.4 and 6.2 ns, respectively) compared to those of their solutions (5.7 and 4.8 ns, respectively), indicating enhanced radiative recombination efficiency in the solid state (Figure 4f). In contrast, the PL lifetime of **TPE3-PTZ** was lower by ca.1 ns in the solid state.

PL quantum yields (PLQY) of the toluene solutions of the compounds were in the range of 3−26%. The highest PLQY was observed for the solution of **TPE3-POZ** (Table 2). PLQYs of the solid samples of the compounds were considerably higher (5.25−53%) than those of the toluene solutions. This observation indicates toward the property of aggregation-induced emission enhancement (AIEE) of the compounds. The significantly higher PLQY of the solutions and of the films

https://doi.org/10.1021/acsaelm.5c00123
ACS Appl. Electron. Mater. XXXX, XXX, XXX−XXX

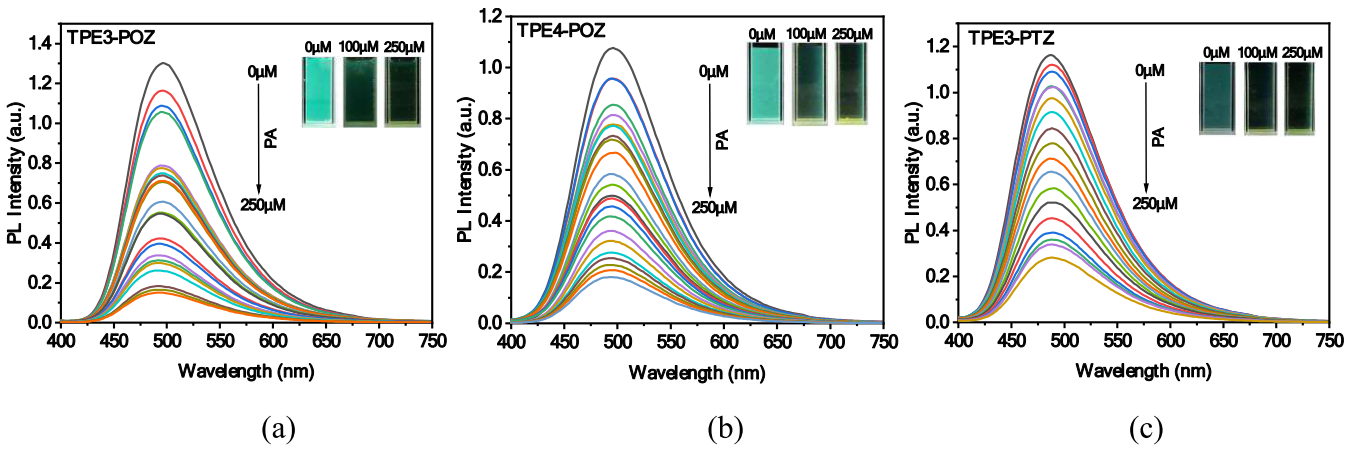

Figure 6. PL spectra of aggregates of **TPE3-POZ** (a), **TPE3-PTZ** (b), and **TPE4-POZ** (c) recorded at the different concentrations of picric acid. Inset pictures of the dispersions containing 0, 100, and 250 μM of picric acid under UV light.

Table 3. Parameters of Picric Acid Detection and of Electroluminescent Devices with TPE3-POZ, TPE4-POZ, and TPE3-PTZ

parameter	stern−volmer constant, ($\times 10^4$ M^{-1})	turn-on voltage (V)[a]	maximum brightness (cd/m^2)[b]	current efficiency (cd/A)[c]	power efficiency (lm/W)[c]	external quantum efficiency (%)[c]	EL maxima (nm)[d]	CIE coordinates (x, y)[d]
TPE3-POZ	2.96	5.5	1900	20.7/19.1	6.8/6.3	6.8/6.3	496/516	0.21, 0.46
TPE4-POZ	2.06	4.3	1700	17.8/17	8.3/7.0	6.7/6.4	494/515	0.20, 0.44
TPE3-PTZ	1.19	5.3	1050	11.2/9.6	3.5/3.4	3.7/3.2	477[e]/501	0.20, 0.39

[a]at 10 cd/m^2. [b]at 10 mA/cm^2. [c]maximum/at 1000 cd/m^2. [d]at 8 V. [e]shoulder.

of **TPE3-POZ**, relative to those of the other derivatives under investigation, can be attributed to its distinct electronic and structural characteristics. The excited-state analyses suggest that **TPE3-POZ** exhibits a slightly reduced dihedral angle between its molecular subunits compared to those of its counterparts. This comparatively less twisted geometry likely facilitates superior molecular packing in the solid film. Such optimized packing minimizes nonradiative decay pathways and enhances radiative recombination efficiency, thereby culminating in its markedly higher PLQY.

2.7. Aggregation-Induced Emission Enhancement and Picric Acid Detection. To validate the aggregation-induced emission enhancement (AIEE) properties of the compounds, the PL spectra of their dispersions in THF−water mixtures with water fractions (f_w) ranging from 0 to 99% were systematically investigated (Figure 5). For the dispersions of **TPE3-POZ**, the emission intensity decreased steadily with a concomitant red shift as the f_w% increased from 0 to 70%. However, at $f_w \geq 80\%$, a significant enhancement in emission intensity was observed, reaching its maximum at f_w of 99%. For the dispersions of **TPE4-POZ** and **TPE3-PTZ**, the emission intensity showed a consistent decrease accompanied by a slight red shift up to an f_w of 60%. Beyond 70% water content, **TPE4-POZ** displayed a marked surge in emission intensity, indicative of robust AIEE. For the dispersions of **TPE3-PTZ**, the increase in emission intensity beyond f_w of 70% was more gradual, with the maximum intensity observed at f_w of 99%. The observed decrease in PL intensity, accompanied by a slight red shift of the emission peak extending up to f_w of 70% for the dispersions of **TPE3-POZ** and up to f_w of 60% for the dispersions of **TPE4-POZ** and **TPE3-PTZ** can be attributed to the twisted intramolecular CT effect.[32] This spectral red shift aligns with the progressive enhancement of CT character as the medium polarity increases. At higher f_w%, the pronounced increase in PL intensity is observed alongside the blue shift of emission. This observation can be ascribed to the increased hydrophobic interactions that drive molecular aggregation.[33] As the aggregation progresses, the effect of the surrounding polar medium is decreased, weakening the intramolecular CT and blue shifting the emission peak. Moreover, aggregation-induced restriction of molecular conformational freedom suppresses nonradiative decay pathways by inhibiting geometric relaxation, thereby significantly enhancing the PL intensity.[34] Notably, the wavelengths of emission maxima of the highly aggregated state (f_w of 99%) for all of the compounds closely matched those observed in PL spectra of the solid samples. This alignment suggests that the photophysical properties of the aggregated forms resemble those of the compounds in their neat solid states. Additionally, as aggregates began forming, the emission spectra exhibited a subtle blue shift. This blue shift indicates minimal self-polarity in the aggregated state, consistent with the emission observed for the solid films (Figure 4e).

Organic luminophores capable of AIEE are highly suited for the detection the nitroaromatic explosive compounds such as picric acid, which are extremely electron-deficient. Aggregates of electron-rich organic compounds interact noncovalently with picric acid, which results in the significant quenching of their emission.[35] The investigated compounds, exhibiting considerable AIEE and the pronounced electron-donating character, were evaluated as potential sensors for picric acid. The aggregates formed at 99% water fraction (f_w% = 99) were selected for this study, as this condition yields the maximum emission intensity due to optimal aggregation. Picric acid, added incrementally at concentrations ranging from 0 to 250 μM, induced progressive quenching of emission, as shown in

https://doi.org/10.1021/acsaelm.5c00123
ACS Appl. Electron. Mater. XXXX, XXX, XXX−XXX

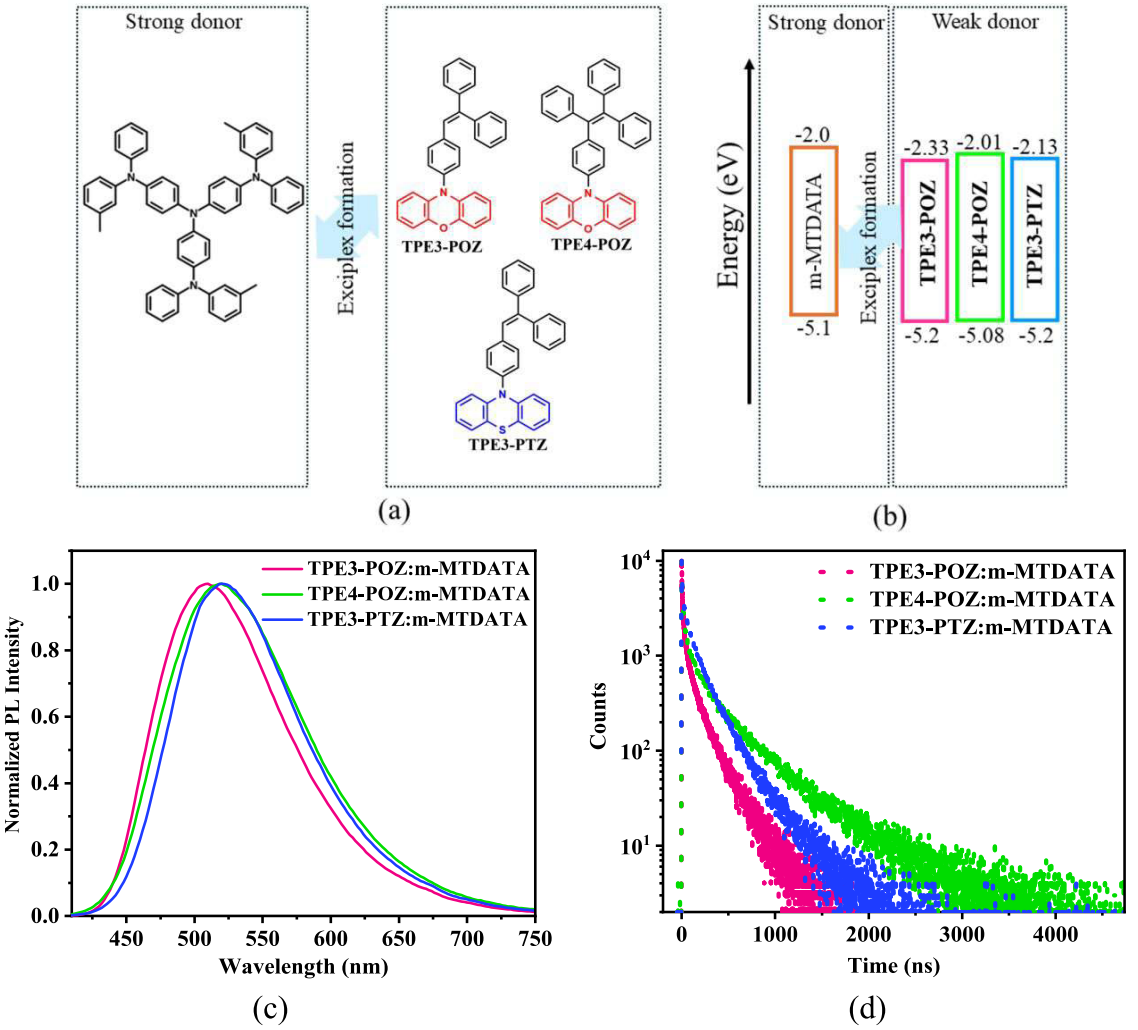

Figure 7. Molecular structures of exciplex-forming compounds and schematic representation of their energy diagrams (a, b), PL spectra (c), and PL decay curves (d) of the molecular mixtures **TPE3-POZ**/m-MTDATA, **TPE4-POZ**/m-MTDATA, and **TPE3-PTZ**/m-MTDATA.

Figure 6. The quenching was pronounced, with substantial fluorescence attenuation observed even at the concentration of picric acid of 100 μM.

The quenching efficiency was quantified using Stern−Volmer plots. The corresponding Stern−Volmer constants (K_{SV}) were determined (Figure S4). The dispersion of **TPE3-POZ** exhibited the highest sensitivity, with a K_{SV} value of 2.96 × 10^4 M^{-1}, followed by that of **TPE4-POZ** (K_{SV} = 2.06 × 10^4 M^{-1}). The dispersion of **TPE3-PTZ** demonstrated the lowest sensitivity, with a K_{SV} of 1.19 × 10^4 M^{-1} (Table 3). This trend correlates with the emission intensities of the solid-state aggregates. The emission of **TPE3-POZ**, with its uniquely structured aggregates and the highest PLQY, exhibited the strongest sensitivity to picric acid. Theoretical investigations employing the mPW1PW91/6−31G(d,p) level, in conjunction with the conductor-like polarizable continuum model (CPCM) using water as solvent, were conducted to precisely model the experimental conditions. Computational investigations provide insights into the quantum chemical interactions between the compounds and picric acid. The optimized geometries and orbital spatial orientations of the complexes of the compounds and picric acid (Figure S5) revealed distinct charge-transfer interactions. A rigorous evaluation of the interatomic distances between the emissive compounds (**TPE3-POZ**, **TPE4-POZ**, and **TPE3-PTZ**) and picric acid reveals the presence of multiple short-range contacts. The detailed structural assessment, provided in Annex (Supporting Information), underscores the existence of noncovalent interactions. In these complexes, hydrogen atoms of electron-rich donors of the studied compounds exhibit extreme short contact with the electron-deficient nitro groups of picric acid indicating noncovalent interaction sites. The HOMO of **TPE3-POZ** and **TPE4-POZ** was localized on the phenoxazine moiety, while that of **TPE3-PTZ** was confined to phenothiazine fragment. In all cases, the LUMO resided on the electron-deficient picric acid. This orbital configuration facilitates smooth charge transfer between the donor (the studied compound) and acceptor (picric acid) mediated by noncovalent interactions. The photoinduced electron transfer (PET) mechanism governing the interaction between the synthesized donor molecules and picric acid is unequivocally supported by DFT calculations at the mPW1PW91/6−31G(d,p) level. The computational analysis reveals the formation of a charge-separated state, where upon excitation, the emissive donor undergoes electron transfer to picric acid, disrupting radiative recombination pathways. This charge-transfer interaction results in a nonradiative relaxation process, effectively quenching fluorescence.[36] The theoretical

https://doi.org/10.1021/acsaelm.5c00123
ACS Appl. Electron. Mater. XXXX, XXX, XXX−XXX

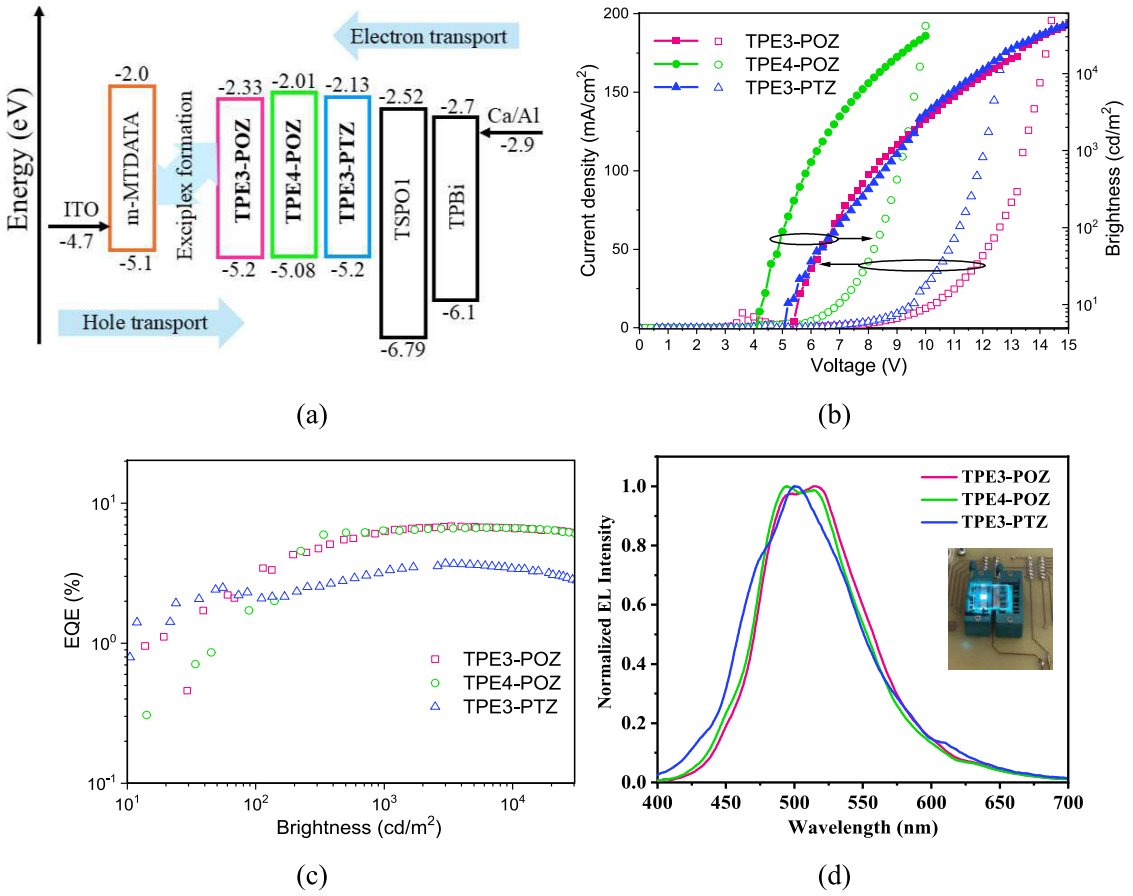

Figure 8. Equilibrium energy diagrams (a) of devices **TPE3-POZ, TPE4-POZ**, or **TPE3-PTZ**; the plots of current density and brightness versus voltage (b) and EQE versus brightness (c); and normalized EL spectra (d) recorded at 8 V. The inset shows the picture of device TPE4-POZ under applied voltage of 8 V.

insights, combined with the experimental photoluminescence studies, provide compelling evidence of PET-driven exciton deactivation, validating the role of noncovalent charge transfer in modulating emission properties.

2.8. Exciplex-Forming Properties. One more advantage of phenylethenyl-substituted phenoxazine and phenothiazine derivatives is their exciplex-forming properties. Despite the weak electron-donating abilities of **TPE3-POZ, TPE4-POZ**, and **TPE3-PTZ**, they formed exciplexes with exciplex-forming donor m-MTDATA in solid-state (Figure 7a,b). The formation of donor−donor exciplexes was detected for the molecular mixtures **TPE3-POZ**/m-MTDATA, **TPE4-POZ**/m-MTDATA, and **TPE3-PTZ**/m-MTDATA with the molar mass ratio of 1:1. In contrast to that of many donor−acceptor exciplexes with significantly red-shifted PL spectra in comparison to the PL spectra of the donor and acceptor,[37−40] the emission bands of exciplexes (509 nm for **TPE3-POZ**/m-MTDATA, 509 nm for **TPE4-POZ**/m-MTDATA, and 519 nm for **TPE3-PTZ**/m-MTDATA) were only slightly red-shifted in comparison to emission spectra of **TPE3-POZ** (495 nm), **TPE4-POZ** (494 nm), and **TPE3-PTZ** (488 nm), respectively (Figure 4e, 7c). The exciplex formation is evident according to PL decay curves of the solid molecular mixtures of **TPE3-POZ, TPE4-POZ**, and **TPE3-PTZ** with MTDATA, which reach the range of microseconds (Figure 7d). PL decay curves of **TPE3-POZ, TPE4-POZ**, and **TPE3-PTZ** are in the nanosecond range (Figure 4f). The long-lived emissions of the molecular mixtures of the studied compounds with m-MTDATA can be explained by exciplex formation between the stronger and weaker donors (Figure 7b). The long-lived emissions of exciplexes are sensitive to oxygen, showing the contribution of triplets to singlet emissions via reverse intersystem crossing causing exciplex-sourced TADF (Figure S6).[41] Strong donor m-MTDATA and weak donors **TPE3-POZ, TPE4-POZ**, and **TPE3-PTZ** have similar I_p^{PE} and E_A^{PE} values in the ranges of 5.1−5.2 and 2.01−2.33 eV, respectively (Figure 7b). As a result, the bands of exciplex emissions are only slightly red-shifted relative to the PL bands of the films of **TPE3-POZ, TPE4-POZ**, and **TPE3-PTZ**. Such exciplex-forming properties of **TPE3-POZ, TPE4-POZ**, and **TPE3-PTZ** can be exploited for efficiency enhancement of OLEDs by triplet harvesting abilities of TADF exciplexes.[42] Such a possibility is discussed in the next section.

The fitting data for PL decay curves and PLQY values of the molecular mixtures of **TPE3-POZ, TPE4-POZ**, and **TPE3-PTZ** with m-MTDAT are collected in Tables S5 and S6. The fittings for the PL decay curves were provided using the formula $y = A1*\exp(-x/\tau_1) + A2*\exp(-x/\tau_2) + A3*\exp(-x/\tau_3)$, where x is τ, A1, A2, and A3 are the fractional intensities of prompt and delayed fluorescence. τ_1 is the lifetime of prompt fluorescence, and τ_2 and τ_3 are lifetimes of delayed fluorescence.[43] The formula

$$\tau = \frac{\sum A_i \tau_i^2}{\sum A_i \tau_i}$$

https://doi.org/10.1021/acsaelm.5c00123
ACS Appl. Electron. Mater. XXXX, XXX, XXX−XXX

was used for the calculation of the average delayed fluorescence lifetimes.[44] The results are shown in Table S7. The lifetimes of prompt fluorescence in air and vacuum were found to be close for **TPE3-POZ**/m-MTDATA, **TPE4-POZ**/m-MTDATA, and **TPE3-PTZ**/m-MTDATA. In contrast, the lifetimes of delayed fluorescence of the samples increased after evacuation. This observation indicates the contribution of triplet excited states to the emissions of the molecular mixtures of the studied compounds with m-MTDATA. To further elucidate the excitonic landscape and triplet harvesting potential, fluorescence and phosphorescence spectra of the most promising exciplex-forming molecular mixture of **TPE4-POZ:m** and **MTDATA**, were recorded at 77 K (Figure S6g). The excited-state dynamics of this exciplex-forming molecular mixture were further probed through temperature-dependent photoluminescence (PL) decay measurements, providing deeper insights into the interplay between singlet and triplet excited states (Figure S6h). The singlet and triplet energies (S_1 and T_1) were determined from the onsets of the fluorescence and phosphorescence spectra recorded at 77 K (Figure S6g). The analysis revealed the exceptionally narrow ΔE_{ST} of 0.07 eV, indicative of a favorable reverse intersystem crossing (RISC). This observation is further supported by the temperature-dependent PL decay curves (Figure S6h), which show an increase of the intensity of delayed fluorescence with rising temperature. This observation provides strong evidence of efficient triplet harvesting via RISC.

2.9. Electroluminescent Devices. Elaborating on efficient doping-free OLEDs, we proposed a unique approach for the efficiency enhancement of OLEDs, combining AIEE and exciplex-forming properties of **TPE3-POZ**, **TPE4-POZ**, and **TPE3-PTZ** in the device structure. Thus, synthesized compounds were tested as emitters of host-free OLEDs using device structure ITO/m-MTDATA (30 nm)/light-emitting layer (20 nm)/TSPO1 (8 nm)/TPBi (30 nm)/Ca (10 nm)/Al (100 nm). The light-emitting layers of **TPE3-POZ**, **TPE4-POZ**, or **TPE3-PTZ** were used in OLEDs named **TPE3-POZ**, **TPE4-POZ**, or **TPE3-PTZ**, respectively. All the functional layers, except the light-emitting layers, were deposited simultaneously for all devices. The devices contained exciplex-forming interfaces **TPE3-POZ**/m-MTDATA, **TPE4-POZ**/m-MTDATA, and **TPE3-PTZ**/m-MTDATA. The layer of diphenyl[4-(triphenylsilyl)phenyl]phosphine oxide (TSPO1) was used for preventing leakage of holes and excitons at interfaces of the studied emitters. The layers of TSPO1 were used taking into account the high ionization potential (6.78 eV) and high triplet energy (3.36 eV) of TSPO1.[45] The layer of 2,2′,2″-(1,3,5-benzenetriyl)-tris(1-phenyl-1-H-benzimidazole) (TPBi) allowed the electron transport from cathode Ca/Al to the light-emitting layer (Figure 8a). Device **TPE4-POZ** showed the lowest turn-on voltage of 4.3 V at 10 cd/m^2 due to the lowest ionization potential of 5.08 eV of **TPE4-POZ** (Figure 8b, Table 3). At the same voltages, devices **TPE3-POZ**, **TPE4-POZ**, and **TPE3-PTZ** reached very different current densities, which is an indication of the different charge-transporting properties of the emitters. **TPE4-POZ** is characterized by superior charge-transporting properties relative to compounds **TPE3-POZ** and **TPE3-PTZ**. Device **TPE4-POZ** showed a current density of 10 mA/cm^2 at a lower voltage (6.6 V) than devices **TPE3-POZ** and **TPE3-PTZ** (at 9.7 and 9.1 V, respectively). As a result, the highest power efficiency of 8.3 lm/W was obtained for device **TPE4-POZ** (Figures S7−9, Table 3). However, the highest current and external quantum efficiencies of 20.7 cd/A and 6.8% were observed for device **TPE3-POZ**. This result agrees with the highest PLQY value of 53% observed for the film **TPE3-POZ** (Table 2). Using the formula

$$\eta_{ext} = \gamma \times \text{PLQY} \times \chi \times \eta_{out}$$

where the charge-balance factor (γ) equals unity, the efficiency of exciton production (χ) equals 0.25 without triplet harvesting ability or unity in the case of triplet harvesting ability, and the outcoupling efficiency (η_{out}) equals 0.3,[46] the theoretical maximum EQE values can be estimated. For OLED **TPE3-POZ** without triplet harvesting ability (χ equals to 0.25), it is of 4%. With the triplet harvesting ability (χ equals unity), the theoretical maximum EQE for device **TPE3-POZ** is of 16% The experimental maximum EQE value of 6.8% observed for device **TPE3-POZ** suggests the possibility of triplet harvesting. The fluorescent emitter **TPE3-POZ** cannot be responsible for the triplet harvesting. We attribute this function to the exciplex-forming interface **TPE3-POZ**/m-MTDATA. It should be noted that the maximum EQE value of devices **TPE3-POZ**, **TPE4-POZ**, and **TPE3-PTZ** were obtained at higher current densities than 10 mA/cm^2, thus at higher brightnesses than 1000 cd/m^2 (Figure 8c). This observation can be explained by the different positions of the zones of recombination from the exciplex-forming interfaces which manifest at low and high current densities. When the recombination zone is located near the exciplex-forming interfaces (Figure 8a), the highest device efficiency is observed. Due to the triplet harvesting by exciplexes, the efficiency roll-offs are negligible at high brightnesses (Figure 8c).

Electroluminescent (EL) spectra of devices **TPE3-POZ**, **TPE4-POZ**, and **TPE3-PTZ** are close to the PL spectra of corresponding emitters (Figures 4b and 8d). In contrast to the structureless PL spectra, structured EL spectra were recorded for the devices. Their EL spectra are characterized by two peaks or one maximum and a shoulder (Table 3). This observation can be attributed to the overlapping of emissions of **TPE3-POZ**, **TPE4-POZ**, and **TPE3-PTZ** and their exciplexes under electrical excitation. The devices exhibited sky blue-greenish-blue electroluminescence (Figures 8d and S7−9, insets). The corresponding International Commission on Illumination (CIE1931) color coordinates are 0.21, 0.46 for **TPE3-POZ**, 0.20, 0.44 for **TPE4-POZ**, and 0.20, 0.39 for **TPE3-PTZ**, respectively (Table 3).

3. CONCLUSIONS

Three phenylethylene derivatives functionalized with phenoxazine and phenothiazine moieties were synthesized and characterized as multifunctional materials for both OLEDs and picric acid sensing applications. The comprehensive computational analyses at the mPW1PW91/6−31G(d,p) level provided profound insights into the ground- and excited-state properties, elucidating the spatial localization and charge-transfer nature of the excited states of the compounds. Photophysical investigations revealed a pronounced aggregation-induced emission enhancement (AIEE) as evidenced by the significantly higher photoluminescence quantum yields (PLQY) of the solid samples (5.25−53%) relative to those of the toluene solutions (3−26%). AIEE was further corroborated by investigation of emission spectra of the dispersions of the compounds in water/THF mixtures. The formation of robust aggregates was observed beyond the water fraction of 60−70%, culminating in peak emission intensities at

https://doi.org/10.1021/acsaelm.5c00123
ACS Appl. Electron. Mater. XXXX, XXX, XXX−XXX

the water fraction of 99%. The solid-state emission spectra with maxima observed between 488 and 495 nm aligned with the spectra of aggregates. The emission of electron-rich and highly emissive aggregates exhibited exceptional sensitivity toward picric acid. It is attributed to noncovalent charge-transfer interactions, as confirmed by both experimental Stern−Volmer analysis and theoretical investigations. The trend in picric acid sensitivity directly correlated with PLQY, highlighting the pivotal role of aggregate emissivity in molecular sensing. OLEDs fabricated using these fast-fluorescent materials as emitters demonstrated cyan electroluminescence with outstanding performance metrics, including luminance exceeding 1000 cd/m^2 and external quantum efficiency (EQE) reaching 6.8%. The relatively high EQE is explained by triplet harvesting from the interface donor−donor exciplexes These results underscore the potential of these phenylethylene derivatives as dual-functional materials, seamlessly integrating high-efficiency luminescence and optical sensing capabilities.

4. EXPERIMENTAL SECTION

4.1. Methods and Instrumentation. *4.1.1. Identification of Molecular Structures.* ^{1}H NMR and ^{13}C NMR spectra were recorded with Bruker Avance III [400 MHz (^{1}H), 100 MHz (^{13}C)] spectrometers at room temperature. All of the data are given as chemical shifts δ (ppm) downfield from Si(CH$_3$)$_4$. Infrared (IR) spectra were recorded using the PerkinElmer Spectrum GX II FT-IR System. The samples of the solid compounds prepared in the form of KBr pellets. Mass spectra (MS) were obtained on the Waters SQ Detector 2.

4.1.2. Thermal Analyses. Differential scanning calorimetry (DSC) measurements were recorded in nitrogen atmosphere with a PerkinElmer at DSC 8500 equipment at a heating rate of 10 °C/min. Thermogravimetric analysis (TGA) was executed on a PerkinElmer TGA 4000 apparatus in a nitrogen atmosphere at a heating rate of 20 °C/min. Melting points were measured with an electrothermal MEL-TEMP melting point apparatus.

4.1.3. Single-crystal X-ray Diffraction. The single crystals for X-ray diffraction analysis of 10-(4-(2,2-diphenylvinyl)phenyl)-10H-phenothiazine (**TPE3-PTZ**) were obtained by slow evaporation technique using mixtures of solutions. The crystals were mounted on the glass stick using glue. The crystallographic analysis was performed employing an XtaLAB mini diffractometer (Rigaku) with graphite monochromated Mo Kα (λ = 0.71075 Å) X-ray source. The measurements were performed at room temperature. The crystallographic data for **TPE3-PTZ** structures reported in this paper have been deposited in Cambridge Crystallographic Data Centre with respective CCDC no (2428286).

4.1.4. Photophysical Investigations. Absorption spectra of dilute (10^{-5} M) solutions in toluene and films registered on a UV−vis−NIR spectrophotometer Lambda 950 (PerkinElmer). Fluorescence spectra and fluorescence quantum yields of dilute solutions in toluene (10^{-5} M) or solid films of the compounds were registered with Edinburgh Instruments LS980 spectrometer.

4.1.5. Electrochemical Study. *Cyclic voltammetry* (*C*−*V*) measurements were recorded using a micro-Autolab III (Metrohm Autolab) potentiostat equipped with a standard three-electrode configuration. A three-electrode cell equipped with a glassy carbon-working electrode, an Ag/AgNO$_3$ (0.01 M in anhydrous acetonitrile) reference electrode, and a Pt wire counter electrode was employed. The measurements were carried out in anhydrous dichloromethane with tetrabutylammonium hexafluorophosphate (0.1 M) as supporting electrolyte under nitrogen atmosphere at a scan rate of 0.05 V/s. The measurements were calibrated using an internal standard, ferrocene/ferrocenium (Fc) system. Oxidation potentials ($E_{1/2}$ vs Fc) for reversible oxidation were collected as average values of the anodic and cathodic peak potentials, Epa and Epc, respectively.

4.1.6. Electroluminescent Devices. Glass substrates with an optically transparent electrode, indium tin oxide (ITO), were used for OLED fabrications. The functional layers were deposited in a vacuum (ca. 2 × 10^{-5} mBar). The OLED active area was 6 mm^2. Electrometer HP4145A and calibrated photodiode were used to record density−voltage and brightness−voltage characteristics. The Ocean Optics USB2000 spectrometer was used to record the electroluminescence spectra of the fabricated devices.

4.2. Materials and Synthesis. All of the required chemicals, i.e., 2-(4-bromophenyl)-1,1-diphenylethenylene, 2-(4-bromophenyl)-1,2,2-triphenylethenylene, solution of tri-*tert*-butylphosphine in toluene (1.00 M), sodium-*tert*-butoxide, palladium acetate, phenoxazine, and phenothiazine, were obtained from Sigma-Aldrich and used as received.

*4.2.1. 10-(4-(2,2-Diphenylethenyl)phenyl)-phenoxazine (**TPE3-POZ**).* Phenoxazine (0.7 g, 5.46 mmol) and 2-(4-bromophenyl)-1,1-diphenylethylene (1.53 g, 6.55 mmol) were dissolved in dry toluene (10 mL) under argon atmosphere. Sodium-*tert*-butoxide (0.73 g, 10.92 mmol), palladium acetate (0.02 g, 0.11 mmol), and tri-*tert*-butylphosphine (1.00 M, 0.02 mL, 0.11 mmol) were added to the solution and the mixture was refluxed for 12 h. When the reaction was finished (TLC control), the mixture was cooled down to room temperature and extracted with ethyl acetate. The organic extract was washed with water and dried (Na$_2$SO$_4$). Then, the solvent evaporated under vacuum. The product was purified by silica gel column chromatography using hexane as an eluent. Yellow crystals were obtained after recrystallization from hexane with a yield of 75% (1.26 g). Mp = 141−143 °C. MS (ES$^+$), m/z = 437 [M]$^+$. ^{1}H NMR (400 MHz, DMSO-d_6) δ (ppm): 5.79−5.84 (m, 2H), 6.63−6.68 (m, 4H), 6.69−6.73 (m, 2H), 7.18 (d, J = 8.4 Hz, 2H), 7.21 (d, J = 7.3 Hz, 3H), 7.28 (d, J = 8.4 Hz, 2H), 7.30−7.50 (m, 8H). ^{13}C NMR (100 MHz, DMSO-d_6) δ (ppm): 113.54, 115.74, 121.91, 124.17, 127.23, 127.62, 128.33, 128.89, 129.55, 130.14, 130.45, 132.42, 134.22, 137.13, 137.85, 140.14, 142.73, 143.32, 143.57. IR ν_{max} (KBr): 3059, 3024 (C−H, Ar); 1622, 1590 (C═C, Ar); 1483, 1462 (C$_6$H$_5$−); 1327; 1263 (C−N−, Ar); 1208 (−C−O-C−); 751, 737 (C═C−H); 695 (CH═CH).

*4.2.2. 10-(4-(1,2,2-Triphenylethenyl)phenyl)-phenoxazine (**TPE4-POZ**).* Compound **2** was prepared by the similar procedure as compound **1**, using phenoxazine (0.40 g, 5.43 mmol), 2-(4-bromophenyl)-1,1,2-triphenylethylene (1.07 g, 6.55 mmol), sodium-*tert*-butoxide (0.42 g, 10.92 mmol), palladium acetate (0.02 g, 0.11 mmol), and solution of tri-*tert*-butylphosphine in toluene (1.00 M, 0.02 mL, 0.11 mmol). White crystals were obtained after recrystallization from hexane with a yield of 71% (0.79 g). Mp = 250−253 °C. MS (ES$^+$), m/z = 513 [M]$^+$. ^{1}H NMR (400 MHz, CDCl$_3$) δ (ppm): 5.78 (d, J = 6.4 Hz, 2H), 6.49−6.61 (m, 6H), 6.95−7.01 (m, 7H), 7.03−7.09 (m, 10H), 7.16 (d, J = 8.1 Hz, 2H). ^{13}C NMR (100 MHz, CDCl$_3$) δ (ppm): 113.20, 115.74, 121.23, 123.18, 126.77, 127.65, 127.79, 127.92, 129.97, 131.25, 131.29, 131.41, 133.90, 134.32, 136.80, 140.20, 142.13, 142.56, 143.95, 144.30. IR ν_{max} (KBr): 3045, 3022 (C−H, Ar); 1627, 1591 (C═C, Ar); 1486, 1463 (C$_6$H$_5$−); 1336; 1270 (C−N−, Ar); 1202 (−C−O-C−); 739 (C═C−H); 696 (CH═CH).

*4.2.3. 10-(4-(2,2-Diphenylethenyl)phenyl)-phenothiazine (**TPE3-PTZ**).* Compound **3** was prepared by a similar procedure to compound **1**, using phenothiazine (0.7 g, 5.02 mmol), 2-(4-bromophenyl)-1,1-diphenylethylene (1.41 g, 6.02 mmol), sodium-*tert*-butoxide (0.68 g, 10.04 mmol), palladium acetate (0.02 g, 0.10 mmol), and tri-*tert*-butylphosphine (1.00 M, 0.02 mL, 0.10 mmol). Light yellow crystals were obtained after recrystallization from hexane with a yield of 69% (1.10 g). Mp = 161−164 °C. MS (ES$^+$), m/z = 453 [M]$^+$. ^{1}H NMR (400 MHz, DMSO-d_6) δ (ppm): 6.21 (d, J = 8.1 Hz, 2H), 6.87 (t, J = 7.4 Hz, 2H), 6.95 (t, J = 7.7 Hz, 2H), 7.08 (d, J = 7.4 Hz, 2H), 7.14 (d, J = 8.1 Hz, 2H), 7.20−7.23 (m, 4H), 7.25 (s, 1H), 7.32−7.48 (m, 8H). ^{13}C NMR (100 MHz, DMSO-d_6) δ (ppm): 117.20, 120.76, 123.43, 127.25, 127.59, 127.77, 128.25, 128.30, 128.88, 129.32, 129.54, 130.15, 132.05, 137.01, 139.59, 140.20, 142.77, 143.02, 143.77. IR ν_{max} (KBr): 3054, 3022 (C−H, Ar); 1588,

https://doi.org/10.1021/acsaelm.5c00123
ACS Appl. Electron. Mater. XXXX, XXX, XXX−XXX

1570 (C═C, Ar); 1463, 1442 (C_6H_5-); 1314; 1260, 1241 (C−N−, Ar); 747 (C═C−H); 702 (CH═CH).

4.3. Computational Strategies. The computational study employs density functional theory (DFT) to investigate the electronic properties of the molecules. The mPW1PW91[47] functional combined with the 6−31G(d,p) basis set was utilized, as implemented in the Gaussian software package.[48] Time-dependent DFT (TD-DFT) calculations were also conducted at the same theoretical level (mPW1PW91/6−31G(d,p)) to explore excited-state properties. These computations were performed in a solvent environment model using the integral equation formalism variant of the polarizable continuum model (IEFPCM).[49] The density of states (DOS) analysis based on Mulliken's charge distribution method,[50] crucial for understanding the distribution of electronic energy levels, was visualized using the PyMOlyze 1.1 program. Furthermore, Marcus theory[51,52] was employed to calculate the reorganization energy, a critical parameter for evaluating charge mobility. As part of this analysis, the internal reorganization energy for holes was determined using eq 1, enabling a deeper understanding of charge transport processes in the current investigation.

$$\lambda_h = [E_+^0 - E_0] + [E_0^+ - E_+] \quad (1)$$

In the above equation, E_+ and E_+^0 are the cationic and neutral energies of cationic geometrical optimization, respectively, and E_0^+ and E_0 are the cationic and neutral energies of neutral optimized geometry, respectively.

■ ASSOCIATED CONTENT

Supporting Information

The Supporting Information is available free of charge at https://pubs.acs.org/doi/10.1021/acsaelm.5c00123.

Detailed descriptions of the synthesis and identification, general experimental information, and additional theoretical and experimental data (PDF)

■ AUTHOR INFORMATION

Corresponding Author

Juozas Vidas Grazulevicius − *Department of Polymer Chemistry and Technology, Kaunas University of Technology, Kaunas 51423, Lithuania;* orcid.org/0000-0002-4408-9727; Email: juozas.grazulevicius@ktu.lt

Authors

Ehsan Ullah Rashid − *Department of Polymer Chemistry and Technology, Kaunas University of Technology, Kaunas 51423, Lithuania;* orcid.org/0009-0005-6725-4085

Monika Cekaviciute − *Department of Polymer Chemistry and Technology, Kaunas University of Technology, Kaunas 51423, Lithuania*

Jurate Simokaitiene − *Department of Polymer Chemistry and Technology, Kaunas University of Technology, Kaunas 51423, Lithuania*

Melika Ghasemi − *Department of Polymer Chemistry and Technology, Kaunas University of Technology, Kaunas 51423, Lithuania;* orcid.org/0000-0003-3342-7310

Dmytro Volyniuk − *Department of Polymer Chemistry and Technology, Kaunas University of Technology, Kaunas 51423, Lithuania;* orcid.org/0000-0003-3526-2679

Khrystyna Ivaniuk − *Lviv Polytechnic National University, Lviv 79013, Ukraine*

Pavlo Stakhira − *Lviv Polytechnic National University, Lviv 79013, Ukraine*

Complete contact information is available at: https://pubs.acs.org/10.1021/acsaelm.5c00123

Author Contributions

E.U.R. and J.V.G. designed the research, E.U.R. performed DFT calculations, M.C. and J.S. performed synthesis, D.V. and M.G. were responsible for the photophysical studies, K.I. and P.S. investigated devices, E.U.R. wrote the manuscript with contribution of all authors, J.V.G. led the project.

Notes

The authors declare no competing financial interest.

■ ACKNOWLEDGMENTS

This project received funding from the Research Council of Lithuania (LMTLT), agreement No. S-LU-24-6. The authors extend their gratitude to Dr. Audrius Bucinskas for his contribution to X-ray diffraction analysis.

■ REFERENCES

(1) Grimsdale, A. C.; Leok Chan, K.; Martin, R. E.; Jokisz, P. G.; Holmes, A. B. Synthesis of Light-Emitting Conjugated Polymers for Applications in Electroluminescent Devices. *Chem. Rev.* **2009**, *109* (3), 897−1091.

(2) Yang, X.; Zhou, G.; Wong, W.-Y. Functionalization of Phosphorescent Emitters and Their Host Materials by Main-Group Elements for Phosphorescent Organic Light-Emitting Devices. *Chem. Soc. Rev.* **2015**, *44* (23), 8484−8575.

(3) Zhao, Z.; Deng, C.; Chen, S.; Lam, J. W. Y.; Qin, W.; Lu, P.; Wang, Z.; Kwok, H. S.; Ma, Y.; Qiu, H. Full Emission Color Tuning in Luminogens Constructed from Tetraphenylethene, Benzo-2, 1, 3-Thiadiazole and Thiophene Building Blocks. *Chem. Commun.* **2011**, *47* (31), 8847−8849.

(4) Mahmoudi, M.; Urbonas, E.; Volyniuk, D.; Gudeika, D.; Dabrovolskas, K.; Simokaitiene, J.; Dabuliene, A.; Keruckiene, R.; Leitonas, K.; Guzauskas, M. Indolocarbazoles with Sterically Unrestricted Electron-Accepting Anchors Showcasing Aggregation-Induced Thermally Activated Delayed Mechanoluminescence for Host-Free Organic Light-Emitting Diodes. *Molecules* **2023**, *28* (16), No. 5999.

(5) Hong, Y.; Lam, J. W. Y.; Tang, B. Z. Aggregation-Induced Emission. *Chem. Soc. Rev.* **2011**, *40* (11), 5361−5388.

(6) Nie, H.; Huang, J.; Zhao, Z.; Tang, B. Z. Aggregation-Induced Emission Luminogens (AIEgens) for Non-Doped Organic Light-Emitting Diodes. In *Aggregation-Induced Emission: Materials and Applications*; ACS Publications, 2016; Vol. *2*, pp 173−198.

(7) Luo, J.; Xie, Z.; Lam, J. W. Y.; Cheng, L.; Tang, B. Z.; Chen, H.; Qiu, C.; Kwok, H. S.; Zhan, X.; Liu, Y.; Zhu, D. Aggregation-Induced Emission of 1-Methyl-1,2,3,4,5-Pentaphenylsilole. *Chem. Commun.* **2001**, 1740−1741.

(8) Luo, J.; Xie, Z.; Lam, J. W. Y.; Cheng, L.; Chen, H.; Qiu, C.; Kwok, H. S.; Zhan, X.; Liu, Y.; Zhu, D. Aggregation-Induced Emission of 1-Methyl-1, 2, 3, 4, 5-Pentaphenylsilole. *Chem. Commun.* **2001**, No. 18, 1740−1741.

(9) An, B. K.; Kwon, S. K.; Jung, S. D.; Park, S. Y. Enhanced Emission and Its Switching in Fluorescent Organic Nanoparticles. *J. Am. Chem. Soc.* **2002**, *124* (48), 14410−14415.

(10) Huang, M.; Lu, H.; Wang, K.; Liu, B.; Wang, M.; Qiao, X.; Yang, J. A Facile Design of Azaanthracene Derivatives: Acq−Aie Conversion and Blue-Shifted Mechanofluorochromic Emission. *Dyes Pigm.* **2021**, *186*, No. 108992.

(11) Huang, J.; Jiang, Y.; Yang, J.; Tang, R.; Xie, N.; Li, Q.; Kwok, H. S.; Tang, B. Z.; Li, Z. Construction of Efficient Blue AIE Emitters with Triphenylamine and TPE Moieties for Non-Doped OLEDs. *J. Mater. Chem. C Mater.* **2014**, *2* (11), 2028−2036.

(12) Li, Y.; Xu, Z.; Zhu, X.; Chen, B.; Wang, Z.; Xiao, B.; Lam, J. W. Y.; Zhao, Z.; Ma, D.; Tang, B. Z. Creation of Efficient Blue Aggregation-Induced Emission Luminogens for High-Performance Nondoped Blue OLEDs and Hybrid White OLEDs. *ACS Appl. Mater. Interfaces* **2019**, *11* (19), 17592−17601.

(13) Li, X.-F.; Chi, Z.-G.; Xu, B.-J.; Li, H.-Y.; Zhang, X.-Q.; Zhou, W.; Zhang, Y.; Liu, S.-W.; Xu, J.-R. Synthesis and Characterization of Triphenylethylene Derivatives with Aggregation-Induced Emission Characteristics. *J. Fluoresc* **2011**, *21*, 1969−1977.
(14) Wang, W.; Lin, T.; Wang, M.; Liu, T.-X.; Ren, L.; Chen, D.; Huang, S. Aggregation Emission Properties of Oligomers Based on Tetraphenylethylene. *J. Phys. Chem. B* **2010**, *114* (18), 5983−5988.
(15) Shi, H.; Xin, D.; Gu, X.; Zhang, P.; Peng, H.; Chen, S.; Lin, G.; Zhao, Z.; Tang, B. Z. The Synthesis of Novel AIE Emitters with the Triphenylethene-Carbazole Skeleton and Para-/Meta-Substituted Arylboron Groups and Their Application in Efficient Non-Doped OLEDs. *J. Mater. Chem. C Mater.* **2016**, *4* (6), 1228−1237.
(16) Cekaviciute, M.; Petrauskaite, A.; Nasiri, S.; Simokaitiene, J.; Volyniuk, D.; Sych, G.; Budreckiene, R.; Grazulevicius, J. V. Towards Blue AIE/AIEE: Synthesis and Applications in OLEDs of Tetra-/Triphenylethenyl Substituted 9, 9-Dimethylacridine Derivatives. *Molecules* **2020**, *25* (3), No. 445.
(17) Mei, J.; Leung, N. L. C.; Kwok, R. T. K.; Lam, J. W. Y.; Tang, B. Z. Aggregation-Induced Emission: Together We Shine, United We Soar! *Chem. Rev.* **2015**, *115* (21), 11718−11940.
(18) Qayyum, M.; Bushra, T.; Khan, Z. A.; Gul, H.; Majeed, S.; Yu, C.; Farooq, U.; Shaikh, A. J.; Shahzad, S. A. Synthesis and Tetraphenylethylene-Based Aggregation-Induced Emission Probe for Rapid Detection of Nitroaromatic Compounds in Aqueous Media. *ACS Omega* **2021**, *6* (39), 25447−25460.
(19) Pervaiz, A.; Shahzad, S. A.; Assiri, M. A.; Javid, T.; Irshad, H.; Khan, K. O. Extensive Optical and DFT Studies on Novel AIE Active Fluorescent Sensor for Colorimetric and Fluorometric Detection of Nitrobenzene in Solid, Solution and Vapor Phase. *Spectrochim Acta A Mol. Biomol Spectrosc* **2024**, *313*, No. 124121.
(20) Du, H.; Zhou, Q.; Yu, Y.; Liu, C.; Zhang, X.; Pang, Z.; Han, S. Observation of Up-Conversion Fluorescence from Exciplex of m-MTDATA:TPBi Blend. *J. Lumin.* **2022**, *243*, No. 118655.
(21) Chapran, M.; Angioni, E.; Findlay, N. J.; Breig, B.; Cherpak, V.; Stakhira, P.; Tuttle, T.; Volyniuk, D.; Grazulevicius, J. V.; Nastishin, Y. A.; Lavrentovich, O. D.; Skabara, P. J. An Ambipolar BODIPY Derivative for a White Exciplex OLED and Cholesteric Liquid Crystal Laser toward Multifunctional Devices. *ACS Appl. Mater. Interfaces* **2017**, *9* (5), 4750−4757.
(22) Sarma, M.; Chen, L. M.; Chen, Y. S.; Wong, K. T. Exciplexes in OLEDs: Principles and Promises. *Mater. Sci. Eng.: R: Reports* **2022**, *150*, No. 100689.
(23) Chapran, M.; Pander, P.; Vasylieva, M.; Wiosna-Salyga, G.; Ulanski, J.; Dias, F. B.; Data, P. Realizing 20% External Quantum Efficiency in Electroluminescence with Efficient Thermally Activated Delayed Fluorescence from an Exciplex. *ACS Appl. Mater. Interfaces* **2019**, *11* (14), 13460−13471.
(24) Hartwig, J. F. Palladium-Catalyzed Amination of Aryl Halides: Mechanism and Rational Catalyst Design. *Synlett* **1997**, *1997* (04), 329−340.
(25) Mitra, S.; Darira, H.; Chattopadhyay, P. Efficient Synthesis of Imidazole-Fused Benzodiazepines Using Palladium-Catalyzed Intramolecular C−N Bond Formation Reaction. *Synthesis (Stuttg)* **2012**, *45* (01), 85−92.
(26) Sych, G.; Simokaitiene, J.; Bezvikonnyi, O.; Tsiko, U.; Volyniuk, D.; Gudeika, D.; Grazulevicius, J. V. Exciplex-Enhanced Singlet Emission Efficiency of Nondoped Organic Light Emitting Diodes Based on Derivatives of Tetrafluorophenylcarbazole and Tri/Tetraphenylethylene Exhibiting Aggregation-Induced Emission Enhancement. *J. Phys. Chem. C* **2018**, *122* (26), 14827−148377.
(27) Kaafarani, B. R.; El-Ballouli, A. O.; Trattnig, R.; Fonari, A.; Sax, S.; Wex, B.; Risko, C.; Khnayzer, R. S.; Barlow, S.; Patra, D.; Timofeeva, T. V.; List, E. J. W.; Brédas, J. L.; Marder, S. R. Bis(Carbazolyl) Derivatives of Pyrene and Tetrahydropyrene: Synthesis, Structures, Optical Properties, Electrochemistry, and Electroluminescence. *J. Mater. Chem. C Mater.* **2013**, *1* (8), 1638−1650.
(28) Sworakowski, J. How Accurate Are Energies of HOMO and LUMO Levels in Small-Molecule Organic Semiconductors Determined from Cyclic Voltammetry or Optical Spectroscopy? *Synth. Met.* **2018**, *235*, 125−130.
(29) Akram, W.; Walayat, A.; Ali Zahid, W.; Peng, T.; Abu El Maati, L.; Alomar, M.; Tawfik, S. G.; Iqbal, J. Molecularly Engineered Pyrrole-Based Hole Transport Materials Featuring Diversified Structures for High-Performance Perovskite Solar Cells from First-Principles. *J. Mol. Liq.* **2024**, *405*, No. 125103.
(30) Nasiri, S.; Cekaviciute, M.; Simokaitiene, J.; Petrauskaite, A.; Volyniuk, D.; Andruleviciene, V.; Bezvikonnyi, O.; Grazulevicius, J. V. Carbazole Derivatives Containing One or Two Tetra-/Triphenylethenyl Units as Efficient Hole-Transporting OLED Emitters. *Dyes Pigm.* **2019**, *168*, 93−102.
(31) Butkute, R.; Masiulyte, A.; Rashid, E. U.; Sargsyan, S.; Moudgalya, N. S.; Leitonas, K.; Volyniuk, D.; Grazulevicius, J. V. Ultralow Dark Current Density of Organic Photodetectors and Organic Light-Emitting Diodes Endowed by Highly Thermally Stable Derivatives of 2,7-Di-Tert-Butyl-9,9-Dimethyl-9,10-Dihydroacridine and Phenanthroimidazole Exhibiting Balanced Bipolar Charge Transport. *ACS Appl. Electron Mater.* **2024**, *6* (6), 4735−4745.
(32) Wang, J.; Yang, Y.; Gu, F.; Zhai, X.; Yao, C.; Zhang, J.; Jiang, C.; Xi, X. Molecular Engineering Modulating the Singlet-Triplet Energy Splitting of Indolocarbazole-Based TADF Emitters Exhibiting AIE Properties for Nondoped Blue OLEDs with EQE of Nearly 20%. *ACS Appl. Mater. Interfaces* **2023**, *15* (51), 59643−59654.
(33) Wang, J.; Yang, Y.; Jiang, C.; He, M.; Yao, C.; Zhang, J. Ultrapure Deep-Blue Aggregation-Induced Emission and Thermally Activated Delayed Fluorescence Emitters for Efficient OLEDs with CIE $y < 0.1$ and Low Efficiency Roll-Offs. *J. Mater. Chem. C Mater.* **2022**, *10* (8), 3163−3171.
(34) Wang, J.; Zhang, J.; Jiang, C.; Yao, C.; Xi, X. Effective Design Strategy for Aggregation-Induced Emission and Thermally Activated Delayed Fluorescence Emitters Achieving 18% External Quantum Efficiency Pure-Blue OLEDs with Extremely Low Roll-Off. *ACS Appl. Mater. Interfaces* **2021**, *13* (48), 57713−57724.
(35) Kachwal, V.; Joshi, M.; Mittal, V.; Choudhury, A. R.; Laskar, I. R. Strategic Design and Synthesis of AIEE (Aggregation Induced Enhanced Emission) Active Push-Pull Type Pyrene Derivatives for the Ultrasensitive Detection of Explosives. *Sens Biosensing Res.* **2019**, *23*, No. 100267.
(36) Kajjam, A. B.; Singh, K.; Tej, R. V. V.; Vaidyanathan, S. Carbazole−Acenaphthene (Donor−Acceptor)-Based Luminophores for Picric Acid Detection: A Combined Experimental and Theoretical Study. *Mater. Adv.* **2021**, *2* (15), 5236−5247.
(37) Guo, J.; Zhen, Y.; Dong, H.; Hu, W. Recent Progress on Organic Exciplex Materials with Different Donor−Acceptor Contacting Modes for Luminescent Applications. *J. Mater. Chem. C Mater.* **2021**, *9* (47), 16843−16858.
(38) Song, X.; Zhang, D.; Li, H.; Cai, M.; Huang, T.; Duan, L. Exciplex System with Increased Donor-Acceptor Distance as the Sensitizing Host for Conventional Fluorescent OLEDs with High Efficiency and Extremely Low Roll-Off. *ACS Appl. Mater. Interfaces* **2019**, *11* (25), 22595−22602.
(39) He, L.; Bai, R.; Yu, R.; Meng, X.; Tian, M.; Wang, X. Donor/Acceptor Pairs Created by Electrostatic Interaction: Design, Synthesis, and Investigation on the Exciplex Formed Within the Pair. *Angew. Chem., Int. Ed.* **2021**, *60* (11), 6013−6020.
(40) Basel, T.; Sun, D.; Baniya, S.; McLaughlin, R.; Choi, H.; Kwon, O.; Vardeny, Z. V. Magnetic Field Enhancement of Organic Light-Emitting Diodes Based on Electron Donor−Acceptor Exciplex. *Adv. Electron Mater.* **2016**, *2* (2), No. 1500248.
(41) Tang, X.; Cui, L. S.; Li, H. C.; Gillett, A. J.; Auras, F.; Qu, Y. K.; Zhong, C.; Jones, S. T. E.; Jiang, Z. Q.; Friend, R. H.; Liao, L. S. Highly Efficient Luminescence from Space-Confined Charge-Transfer Emitters. *Nat. Mater.* **2020**, *19* (12), 1332−1338.
(42) Chapran, M.; Sahalianov, I.; Karaush-Karmazin, N. N.; Wiosna-Salyga, G.; Glowacki, I.; Luszczynska, B.; Pander, P.; Baryshnikov, G. V. Electronic Structure of Exciplexes and the Role of Local Triplet States on Efficiency of Thermally Activated Delayed Fluorescence. *ACS Appl. Electron Mater.* **2023**, *5* (3), 1489−1501.

https://doi.org/10.1021/acsaelm.5c00123
ACS Appl. Electron. Mater. XXXX, XXX, XXX−XXX

(43) Han, C.; Zhang, Z.; Ding, D.; Xu, H. Dipole-Dipole Interaction Management for Efficient Blue Thermally Activated Delayed Fluorescence Diodes. *Chem.* **2018**, *4* (9), 2154−2167.
(44) Sillen, A.; Engelborghs, Y. The Correct Use of "Average" Fluorescence Parameters. *Photochem. Photobiol.* **1998**, *67* (5), 475−486.
(45) Sun, D.; Ren, Z.; Bryce, M. R.; Yan, S. Arylsilanes and Siloxanes as Optoelectronic Materials for Organic Light-Emitting Diodes (OLEDs). *J. Mater. Chem. C Mater.* **2015**, *3* (37), 9496−9508.
(46) Tsutsui, T. Progress in Electroluminescent Devices Using Molecular Thin Films. *MRS Bull.* **1997**, *22* (6), 39−45.
(47) Adamo, C.; Barone, V. Exchange Functionals with Improved Long-Range Behavior and Adiabatic Connection Methods without Adjustable Parameters: The MPW and MPW1PW Models. *J. Chem. Phys.* **1998**, *108* (2), 664−675.
(48) Frisch, M. J.; Trucks, G. W.; Schlegel, H. B.; Scuseria, G. E.; Robb, M. A.; Cheeseman, J. R.; Scalmani, G.; Barone, V.; Petersson, G. A.; Nakatsuji, H.; Li, X.; Caricato, M.; Marenich, A. V.; Bloino, J.; Janesko, B. G.; Gomperts, R.; Mennucci, B.; Hratchian, H. P.; Ortiz, J. V.; Izmaylov, A. F.; Sonnenberg, J. L.; Williams-Young, D.; Ding, F.; Lipparini, F.; Egidi, F.; Goings, J.; Peng, B.; Petrone, A.; Henderson, T.; Ranasinghe, D.; Gao, J.; Rega, N.; Zheng, G.; Liang, W.; Hada, M.; Ehara, M.; Toyota, K.; Fukuda, R.; Hasegawa, J.; Ishida, M.; Nakajima, T.; Honda, Y.; Kitao, O.; Nakai, H.; Vreven, T.; Throssell, K.; Montgomery, J. A.; P, J. E., Jr.; Ogliaro, F.; Bearpark, M. J.; Heyd, J. J.; Brothers, E. N.; Kudin, K. N.; Staroverov, V. N.; Keith, T. A.; Kobayashi, R.; Normand, J.; Raghavachari, K.; Rendell, A. P.; Burant, J. C.; Iyengar, S. S.; Tomasi, J.; Cossi, M.; Millam, J. M.; Klene, M.; Adamo, C.; Cammi, R.; Ochterski, J. W.; Martin, R. L.; Morokuma, K.; Farkas, O.; Foresman, J. B.; Fox, D. J. *Gaussian 16*, revision A.03; Wallingford CT, 2016.
(49) Marenich, A. V.; Cramer, C. J.; Truhlar, D. G. Universal Solvation Model Based on Solute Electron Density and on a Continuum Model of the Solvent Defined by the Bulk Dielectric Constant and Atomic Surface Tensions. *J. Phys. Chem. B* **2009**, *113* (18), 6378−6396.
(50) Mulliken, R. S. Electronic Population Analysis on LCAO−MO Molecular Wave Functions. I. *J. Chem. Phys.* **1955**, *23* (10), 1833−1840.
(51) Brédas, J. L.; Calbert, J. P.; Da Silva Filho, D. A.; Cornil, J. Organic Semiconductors: A Theoretical Characterization of the Basic Parameters Governing Charge Transport. *Proc. Natl. Acad. Sci. U. S. A.* **2002**, *99* (9), 5804−5809.
(52) Shuai, Z.; Li, W.; Ren, J.; Jiang, Y.; Geng, H. Applying Marcus Theory to Describe the Carrier Transports in Organic Semiconductors: Limitations and Beyond. *J. Chem. Phys.* **2020**, *153* (8). DOI: 10.1063/5.0018312/1061733.

https://doi.org/10.1021/acsaelm.5c00123
ACS Appl. Electron. Mater. XXXX, XXX, XXX−XXX